Title	An RCM experimental and modeling study on CH4 and CH4/C2H6 oxidation at pressures up to 160 bar
Author(s)	Ramalingam, Ajoy; Zhang, Kuiwen; Dhongde, Avnish; Virnich, Lukas; Sankhla, Harsh; Curran, Henry J.; Heufer, Alexander
Publication Date	2017-06-13
Publication Information	Ramalingam, Ajoy, Zhang, Kuiwen, Dhongde, Avnish, Virnich, Lukas, Sankhla, Harsh, Curran, Henry, & Heufer, Alexander. (2017). An RCM experimental and modeling study on CH4 and CH4/C2H6 oxidation at pressures up to 160 bar. Fuel, 206, 325-333. doi: https://doi.org/10.1016/j.fuel.2017.06.005
Publisher	Elsevier
Link to publisher's version	https://doi.org/10.1016/j.fuel.2017.06.005
Item record	http://hdl.handle.net/10379/6899
DOI	http://dx.doi.org/10.1016/j.fuel.2017.06.005

An RCM Experimental and Modeling Study on CH_4 and CH_4/C_2H_6 Oxidation at Pressures up to 160 bar

Ajoy Ramalingam[a*], Kuiwen Zhang[b,e], Avnish Dhongde[d], Lukas Virnich[d], Harsh Sankhla[c], Henry Curran[b], Alexander Heufer[a]

[a] *Physico-Chemical Fundamentals of Combustion (PCFC), RWTH Aachen University, Germany*

[b] *Combustion Chemistry Centre, School of Chemistry, NUI Galway, Ireland*

[c] *FEV GmbH, Aachen, Germany*

[d] *Lehrstuhl für Verbrennungskraftmaschinen VKA, RWTH Aachen University, Germany*

[e] *Lawrence Livermore National Laboratory, Livermore, CA, USA*

[*] *Corresponding Author:*
Ajoy Ramalingam
Physico-Chemical Fundamentals of Combustion (PCFC)
RWTH Aachen University, Schinkelstraße 8
52062 Aachen, Germany
Phone: +49 241 80-96241
Fax: +49 241 80-92630
Email: ramalingam@pcfc.rwth-aachen.de

Abstract

The oxidation of CH_4 and CH_4/C_2H_6 mixtures were studied at pressures relevant to knocking in large bore natural gas engines. The experiments were carried out in a rapid compression machine (RCM) at end of compression (EOC) temperatures ranging between 885 – 940 K at compressed gas pressures of 105, 125, 150, and 160 bar at varying equivalence ratios (0.417, 0.526, and 1.0) and dilution percentages (0, 10, and 30% Exhaust Gas Recirculation - EGR) that were defined in a test matrix. This study describes the method and limitations of performing high-pressure experiments of this magnitude in an RCM, modeling, and validation of the kinetic mechanism against experimental data. While the recently published AramcoMech 2.0 could well predict the ignition delay times (IDTs) for CH_4 within the uncertainty ranges at comparatively higher pressures and lower temperatures (885 – 940 K), the predicted reactivity is, in general, lower than that of AramcoMech 1.3 as shown in our previous screening study. Based on the comparison between both mechanisms as well as sensitivity analysis on the predicted IDTs, the reaction rate constant for Ḣ-atom abstraction from CH_4 by $H\dot{O}_2$ radical was optimized in order to achieve better agreement with the new data while maintaining the agreement to the previous data sets. The modified mechanism predicts well the IDTs and the trend of their variation caused by the change in pressure, equivalence ratio, dilution percentage, and mixture variation with C_2H_6.

Keywords: RCM, Methane, Ignition delay, elevated pressures, modeling

1. Introduction

Due to the development of new extraction technologies and falling prices, natural gas is becoming an increasingly popular fuel, especially for commercial engine applications [1]. One of the limiting factors in achieving higher combustion efficiency in large bore commercial engines is the knocking phenomenon in the end-gas (unburnt zone). This can be predicted with the aid of software tools coupled with detailed chemical kinetic mechanisms. An example for one such software chain is the combination of 0-D, 1-D, and 3-D Computational Fluid Dynamics (CFD) tools developed at FEV GmbH in co-operation with the Institute for Combustion Engines, RWTH Aachen University [2]. The conventional combustion strategy for commercial engines (bore < 180 mm) is an open-chamber spark ignited operation mode either with equivalence ratio (ϕ) close to 1 together with EGR or a lean operation mode ($\phi < 0.625$). For large bore engines (bore > 180 mm), a pre-chamber is employed (with or without gas injection), where the natural gas is ignited and the high turbulent jets coming from the pre-chamber then ignite the gas in the main chamber [1]. Typically, the equivalence ratios in the main chamber range from 0.526 to 0.417 and compression end pressures exceed 100 bar at full engine load. The pressure, temperature, and equivalence ratio which are chosen for the investigation of this study, represent the conditions in the end-gas region of the engine at the start of ignition and close to the center of combustion, consequently reflecting real engine application conditions.

A kinetic understanding formulated in kinetic mechanisms are required for today's combustor design tools [2]. Natural gas relevant modeling and experimental studies in this regard have been published previously. The work by Spadaccini et al. [3] covered a comprehensive literature review on natural gas to the 1990's and this study also involved shock tube experiments to determine IDTs for mixtures of methane with ethane, propane, or butane at equivalence ratios of 0.45 – 1.25 at pressures of 3 – 15 bar. There is a large experimental database [3-22] available for IDT shock tube investigations of CH_4 and C_2H_6 at higher temperatures (>1000 K) and pressures varying from 1 to 480 bar. However, for IDT studies at lower temperatures (600 to 1100 K) and comparatively higher pressures (> 40 bar) the available data is sparse [23-29]. The recent work by Aul et al. [16] focused on deriving a test condition based on the statistical design of experiments and it also emphasized the need to validate mechanisms in areas for which little data have been recorded experimentally. Consequently, this study aims to expand the unexplored area of lower

temperatures and elevated pressures for C1 – C2 hydrocarbons at varying equivalence ratios and dilution percentages in an RCM. **Figure 1** shows the graphical insight of the conditions tested with both shock tube and RCM from various studies and the novel targeted regime which is the focus of this paper.

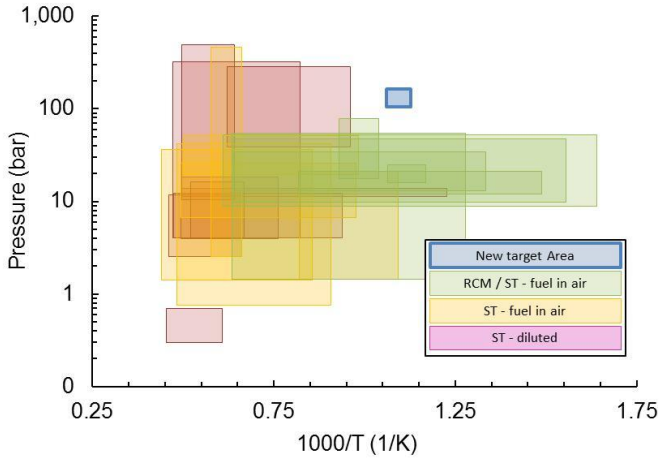

Figure 1: The graphical overview of the literature on Natural gas mixtures for the different targeted pressures and temperatures.

Herein, we deliver a new set of high-pressure experiments for CH_4 and CH_4/C_2H_6 mixtures, which according to the authors' knowledge, are the first set of experiments recorded in an RCM at EOC gas pressures up to 160 bar. It builds upon a previous screening study carried out with CH_4 and CH_4/C_3H_8 mixtures in the same facility at pressures ranging from 80 to 120 bar [30]. The extended pressure and equivalence ratio range cover the relevant conditions of large bore gas engines as described before. These experiments are used for modeling and validating the chemical kinetic mechanism.

2. Experiments

The experiments were performed on a defined test matrix relevant to knocking in the main chamber and pre-chamber of large bore gas engines. The test matrix involves a variation of pressure, dilution, equivalence ratio, and mixture composition. The dilution of the gas mixture was considered in order to reflect the effect of inert EGR. While CO_2 and H_2O are major combustion products found in the exhaust gas, previous studies have shown that their chemical effect is minor. The work of Donohoe et al. [31] showed that there is a significant change in thermal properties of the mixture with steam addition, whereas no relevant chemical effect is observed. Zeng et al. [32] studied the effect of N_2 and CO_2 on the ignition characteristics of CH_4/air mixtures in shock tubes for dilution coefficients of 0%, 20%, and 50%. It was observed that for fuel-lean

mixtures there is a diminutive change in the reactivity when the mixture is diluted by 20% of either N_2 or CO_2. For this reason, the EGR is represented by the percentage of diluent in this study instead of considering CO_2 and H_2O as diluents. **Table 1** shows the test matrix which was used for this study. In order to understand the representation of % EGR with inert gas diluent mol % a brief explanation of the same is attached to the supplementary material.

No.	Pressure	EGR	ϕ	Mole fraction %			
	[bar]	mol %	-	CH_4	C_2H_6	diluent	O_2
1	105	10	0.526	4.74	0	77.26	18.00
2	125	10	0.526	4.74	0	77.26	18.00
3	150	10	0.526	4.74	0	77.26	18.00
4	125	0	0.526	5.24	0	74.86	19.90
5	125	0	0.526	4.17	0.62	75.21	19.99
6	160	30	1	6.63	0	80.13	13.25
7	125	0	0.417	4.19	0	75.69	20.12

Table 1: Test matrix used in the study

The construction of the RCM used in this study has been described in detail by Lee et al. [33]. The facility utilizes a pneumatic driving and hydraulic stopping mechanism, and for these high-pressure experiments both the driving and hydraulic pressure had to be increased substantially. Mixture preparation was carried out in a stainless steel mixing vessel and the partial pressures of individual gases were monitored using two pressure sensors ranging from 0 – 500 mbar (STS ATM.1st) and 0 – 10 bar (STS ATM.1st). The initial temperature was recorded with several type T thermocouples that were mounted on the outer surface of the reaction chamber and the mean value was considered for the initial temperature. The combustion chamber has ports accessible for pressure data acquisition and can withstand pressures up to 1000 bar. For the unconventionally high EOC pressures targeted in this study, special care had to be taken for the pressure measurements. Typically, for low-pressure experiments, a Kistler (6125C-U20) sensor with low thermal shock error is used. However, this Kistler sensor has an overload pressure of only 350 bar which is insufficient to withstand the pressure peaks that occur in this study. For this reason, the reaction chamber was fitted with a PCB sensor (PCB 113B22) for reactive experiments. This has the advantage of having a similar measuring range as that of the Kistler sensor but has a maximum burst pressure of 1034 bar. However, the PCB sensor

104 can be affected by thermal heat shock due to the rapid temperature changes during an experiment. One
105 possible measure to avoid this is by the addition of a thin layer of silicone in front of the sensor but this may
106 influence the ignition behaviour of the test mixture and the layer also depletes quickly because of the harsh
107 conditions of this study. For this reason, the silicone layer was not applied to the PCB sensor during the
108 reactive experiments. Instead, the pressure in the non-reactive experiments were measured using both the
109 Kistler and PCB sensors simultaneously so that, the heat shock effect on the PCB sensor can be quantified
110 and used to correct the pressure measurement of the reactive experiment for each condition. The heat
111 shock effect was quantified by using the ratio of the compressed pressures recorded by the Kistler sensor to
112 that of the PCB sensor for each experiment and further taking the average of the ratios to correct for the
113 amplification factor of the PCB sensor. An example of this procedure is provided in the Supplementary
114 material. The possible uncertainties induced by this method compared to a directly measured pressure are
115 included in the uncertainty analysis presented later. Despite the high burst pressure of the PCB sensor, this
116 sensor was damaged during the first set of experiments. It was speculated that this is due to the very fast
117 pressure increase at ignition inducing high accelerating forces inside the sensor. In order to reduce the peak
118 load on the sensor, the new PCB sensor was afterwards mounted in a recessed configuration in contrast to
119 the Kistler sensor, which was flat mounted during the non-reactive experiments. If the pressure increase is
120 quantified in kbar/ms, the ignition event with the sensor on the flat mounted configuration observed a
121 maximum value of 150 kbar/ms whereas, with the recessed mounting it is about an order of magnitude
122 lower. The recessed mounting configuration degrades the sensor's ability to measure high frequencies and
123 the cavity effect of this configuration will typically reduce the sensor's resonant frequency. However, the
124 pressure traces shown in **Figure 2** illustrate the minor differences in both the flat mounted and recessed
125 configuration. The compression of the gas mixture is a comparatively slow process and the recess
126 configuration used does not influence the pressure measured at the end of compression. The second
127 important parameter to be deduced from the pressure reading is the IDT. As mentioned before, the rate of
128 pressure rise due to the ignition event is reduced when using the recessed configuration and this could, in
129 theory, influence the measured/deduced IDT. However, the difference in the IDT due to the recessed
130 configuration only amounts to less than 0.01 ms and is negligible for the measured range of IDTs. A

comparison of the difference in the IDTs, induced by the two configurations is presented in the Supplementary material. The increase in the dead volume due to the recessed configuration is about 5 µl compared to the smallest EOC volume which is about 34 ml (i.e at the highest compression ratio) and is, therefore, negligible. It is important to note that neither the design influences significantly the measurement of the IDT nor the pressure at EOC, but it reduces the peak pressure levels by a factor of approximately 50%. One also is informed that the change in EOC pressures and temperatures seen in the traces is attributed to the change in initial conditions and is not an effect of the recessed configuration. The rapid rate of pressure drop seen after the ignition event is due to heat loss and possibly also piston rebound and thermal heat shock behavior of the pressure transducer. Since the behaviour after ignition is ~~inessential~~ not essential to this study, we do not ~~more emphasis~~ consider ~~is not given to~~ the pressure traces after the ignition event.

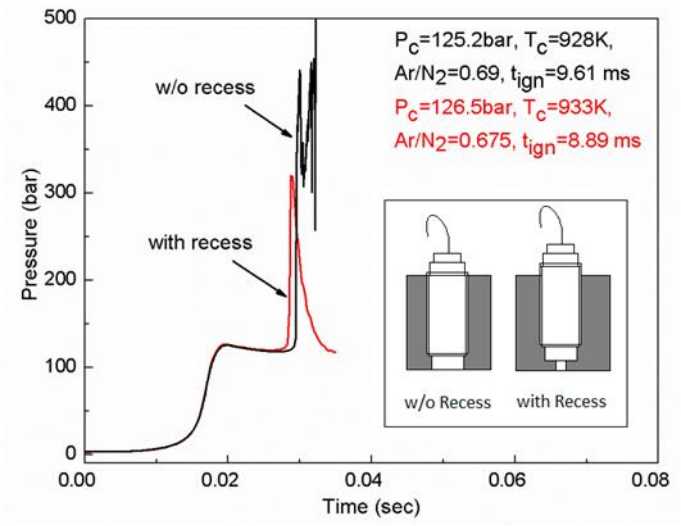

Figure 2: Pressure profile of a reactive experiment with and without recessed adaptor for the pressure sensor (PCB)

To vary the EOC temperature, either the proportion of the diluent gases (Ar/N_2, 0–100%) can be changed, or the end-wall position can be varied (0–21 mm) to change the compression ratio (~7 to 17). The effect of these changes on the heat loss after EOC must be understood. **Figure 3** shows the effect on the heat loss by varying the content of argon in the mixture for a fixed end wall position. The higher the argon content, higher the heat loss, which can be observed by the drop in pressure after the EOC. This effect of different diluent gas composition on the IDTs in an RCM has been discussed previously in more detail by Würmel et al. [34]. As the volume of the reaction chamber decreases with the change in end wall position,

the ratio of volume to surface area also decreases leading to a stronger pressure drop due to heat loss. **Figure 3** also shows the normalized pressure traces for 105, 125 and 150 bar conditions for a specific compressed temperature and it illustrates the effect of heat loss with the change due to end wall position and compression ratio, respectively. The combination of changing the diluent gas and the end-wall position allows one to tailor the experiments to acclimate varying conditions in a test matrix. The EOC temperature was calculated using Gaseq [35] which employs an adiabatic compression/expansion routine and the temperature dependent ratio of specific heats.

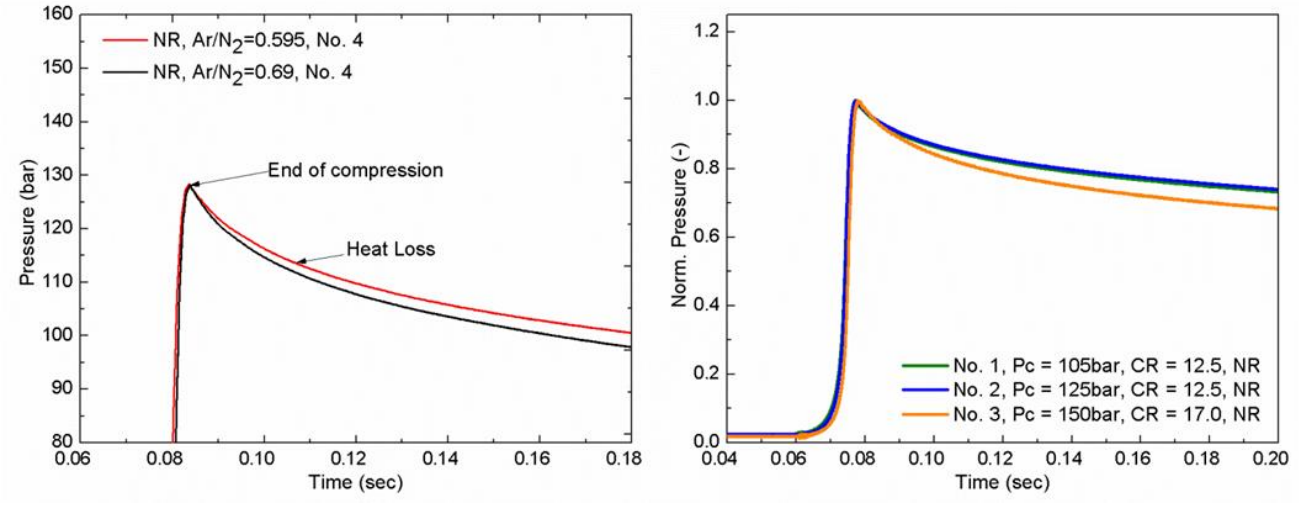

Figure 3: Non-Reactive pressure profile (Kistler) at fixed end wall position and varying Argon content in the methane mixture for 125 bar, ϕ=0.526. Normalized pressure traces of the 105, 125 and 150 bar conditions with different compression ratios.

The measurement uncertainty that would contribute to the calculation of the EOC temperature was estimated for the conditions tested. In the calibrated pressure and temperature range, the PCB and the Kistler sensor have an uncertainty of 0.07% and 0.04% of full scale (FS), respectively. The initial temperature measured with a T type thermocouple has an uncertainty of ±0.5 K. The initial pressure and mixture preparation which were monitored by the two static sensors have an uncertainty of ≤ ± 0.05% of FS. Considering the possible uncertainties in the thermal data of the species, the initial temperature (T_o), initial pressure (p_o), the corresponding change in the equivalence ratio of the prepared mixture ($\Delta\phi$=0.42%), and the measuring uncertainty in the EOC pressure (ΔP_C=±0.15 bar); the combined uncertainty leads to a deviation of ±5 K in the EOC temperature (T_C). A study by Weber et al. [36] focused on the uncertainty estimation of the compressed temperature in an RCM, where scripts to estimate uncertainty using the

independent parameter analysis method and the Monte Carlo method were devised. In the end, Weber et al. reported uncertainties in the compressed temperature for propene at relatively higher pressures (40 bar) in a similar magnitude to those reported here. A comparative estimation of the uncertainty using the method reported here and by Weber et al [36] is available in the Supplementary material. All reactive experiments were repeated once showing good repeatability with a variation in IDT for the majority of the experiments to be within ±4% with only one condition showing ±8% at a constant EOC pressure and temperature. All figures below showing the ignition delay times results ~~in the following visualize~~ indicate this maximum variation of ±8% in our measurements as error bars. Comparatively, in the study of Burke et al. [37] the scatter of experimental data in the two different RCMs (NUIG and UConn) was found to be ±15% and ±10%, respectively. The variation observed in this study lies within this range. The uncertainties in the measurement of the non-reactive experiments are the same as those for ~~at of~~ the corresponding reactive experiments as they utilize the same measuring system. ~~Therefore~~Consequently, the uncertainty in the simulations resulting from using an effective volume profile deduced from a measured pressure profile will also be the same as the measurement uncertainty.

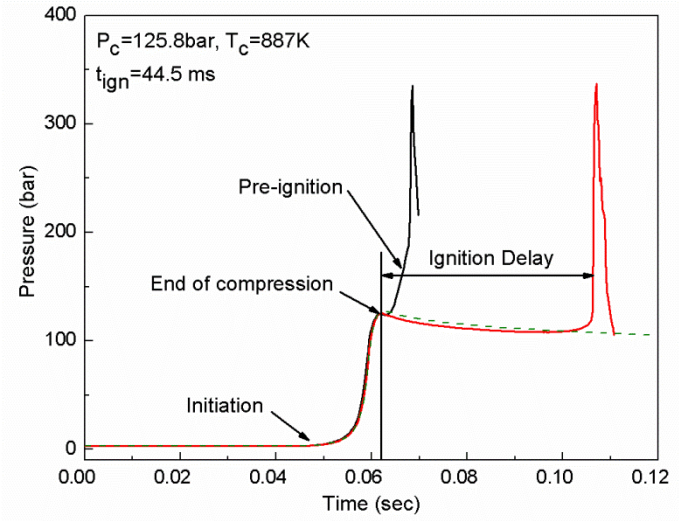

Figure 4: Pressure profile of reactive, non-reactive and a pre-ignition experiment for methane at 125 bar and ϕ=0.526.

The test gases used for this study were of high purity and supplied by Praxair and Westfalen [CH_4, C_2H_6 – 99.95% and for diluent gases Ar – 99.996%, N_2, and O_2 – 99.999%]. **Figure 4** also shows the pressure profile of a 125 bar experiment and its corresponding non-reactive trace. It should be emphasized that during the experimental work, pre-ignition experiments were encountered similar to those observed by

Mittal and Sung [38]. Pre-ignition is an inhomogeneous ignition event leading to a steady increase in pressure before the main ignition. Experiments were first conducted at 125 bar conditions when the pre-ignition occurred and later different pressures and temperatures were scanned to check for the occurrence of pre-ignition. An analysis of these measurements revealed that pre-ignition occurred only at higher pressures but the reason was due to a different factor. It was found that the reaction chamber was contaminated with a thin layer of hydraulic oil which was a consequence of the increase in the hydraulic pressure which was necessary for the high-pressure experiments in this study. A thin shim was introduced between the hydraulic and the reaction chambers, thereby eliminating the ingress of hydraulic oil and reducing the occurrence of pre-ignition. Furthermore, the chamber was cleaned frequently as a precaution. However, occasionally the experiments showed pre-ignition and they were not included for further analysis. **Figure 5** shows the plot of the IDT against the inverse of EOC temperature for the reliable experimental points and the pre-ignition experimental points. In addition, the representative uncertainties in the EOC temperature (±5 K) and variation in the IDT (±8%) are presented in **Figure 5**.

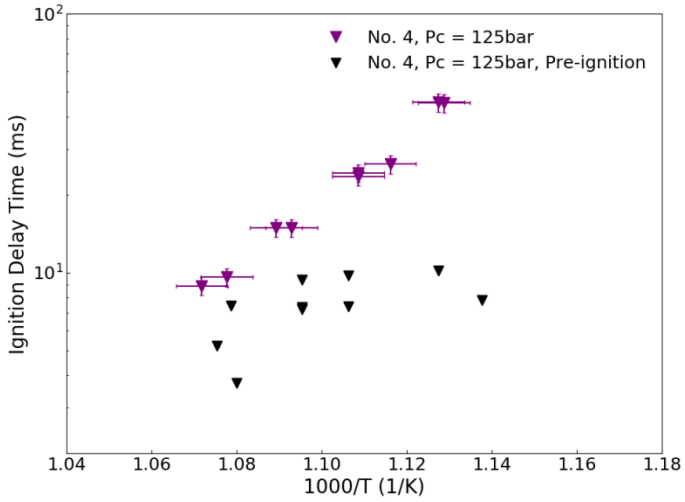

Figure 5: Ignition delay time data and pre-ignition experimental data for methane at 125 bar, ϕ=0.526.

Performing experiments at such high pressures in this facility were primarily limited by the pressure sensors. The design pressure of the reaction chamber is high enough to withstand a higher EOC pressure with similar gas mixtures and the effect of the strong ignition pressure peak on the sensor can be reduced with the recessed arrangement. However, reactive and non-reactive pressure traces of the 150 and 160 bar experiments showed the first signs of oscillations in pressure at EOC, which may be caused either by the

large inertial forces generated when the piston stops, or by the vibration induced by the contact between the pin and groove assembly. To achieve these high-pressure conditions (160 bar), the driver pressure on the pneumatic side had to be increased to 24 bar. Comparing this to the standard EOC pressure conditions (20 bar) the driver pressure typically used is 8–10 bar. A conclusion on the oscillations observed in the high-pressure case is not possible at the moment and further analysis on the dynamics is required. For this reason, EOC pressures higher than 160 bar have not been investigated in this study. A solution to this problem and investigating higher pressures will be considered in future studies.

3. Modeling

The kinetic model used in this work is from the base chemistry up to C_2 species of the recently published AramcoMech 2.0 [39]. Compared to the earlier published AramcoMech 1.3 [40], the most significant change in the base chemistry are the updated rate constants for $H\dot{O}_2+H\dot{O}_2<=>H_2O_2+O_2$ and $\dot{O}H+H\dot{O}_2<=>H_2O+O_2$, which are from Hong et al. [41]. Part of the CH_3O chemistry has been adopted from the recent work of Burke et al. [42] on methanol, including the interactions of $CH_3\dot{O}$ radicals with $\dot{O}H$, $H\dot{O}_2$, H_2O_2 CH_4 and $H\dot{C}O$. Additionally, in the previously published AramcoMech 1.3 [40], the reaction rate constants for $CH_4+H\dot{O}_2<=>\dot{C}H_3+H_2O_2$ were taken from the work of Iparraguirre et al [43] with the A-factor increased by 50%. In AramcoMech 2.0 [39], this value was restored to the value calculated by Iparraguirre et al. [43].

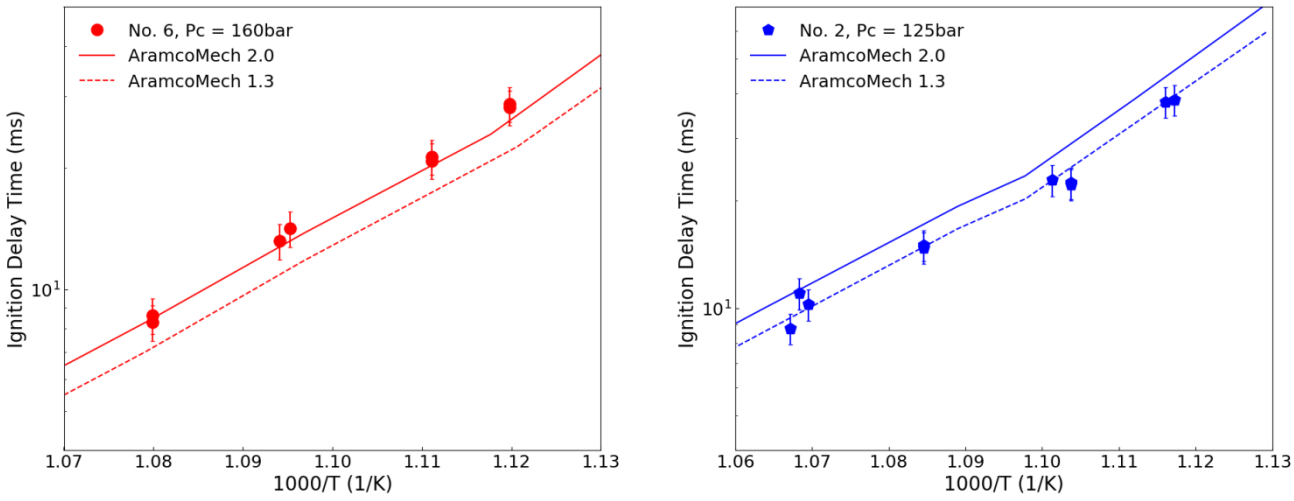

Figure 6: Comparison of experimental data and model predictions at pressures of 160 and 125 bar.

In this work, we found that the predicted IDTs of methane are sensitive to the reaction rate of $CH_4+H\dot{O}_2 <=> \dot{C}H_3+H_2O_2$. **Figure 6** shows that AramcoMech 1.3 [40] in general predicts shorter IDTs than AramcoMech 2.0 [39] and therefore results in an over-prediction of reactivity under some conditions, while the latter tends to under-predict reactivity in some cases.

Through comprehensive comparisons, we found that the best agreement can be achieved by using a value between those from AramcoMech 1.3 [40] and AramcoMech 2.0 [39]. Thus, the A-factor of $CH_4+H\dot{O}_2 <=> \dot{C}H_3+H_2O_2$ in the mechanism used in this work is 25% higher than the value reported by Iparraguirre et al. [43]. The remainder of AramcoMech 2.0 [39] has been used unmodified. Further comparisons of the current mechanism and AramcoMech 1.3 [40] and AramcoMech 2.0 [39] can be found in the Supplementary material, which indicates that these modifications have in general, led to improved model predictions.

4. Results and Discussion

Experiments were performed for the range of conditions listed in Table 1. As mentioned earlier, reactive experiments were carried out using the PCB sensor and the non-reactive experiments used both the PCB and Kistler sensors. For the purpose of simulation, the non-reactive pressure profiles from the Kistler sensor were utilized. Non-reactive pressure traces are essential in capturing the facility effects of the RCM experiments i.e. radical pool generation during the compression phase and heat loss after the EOC, which is detailed in the work of Sung and Curran [44]. In order to extend the simulations beyond the measured experimental range, the initial temperature of the measured non-reactive profiles were changed. The adapted mechanism is used for simulation of IDTs for the various conditions in the test matrix. In addition, the modified mechanism, experimental data, and the corresponding non-reactive profiles are included in the Supplementary material.

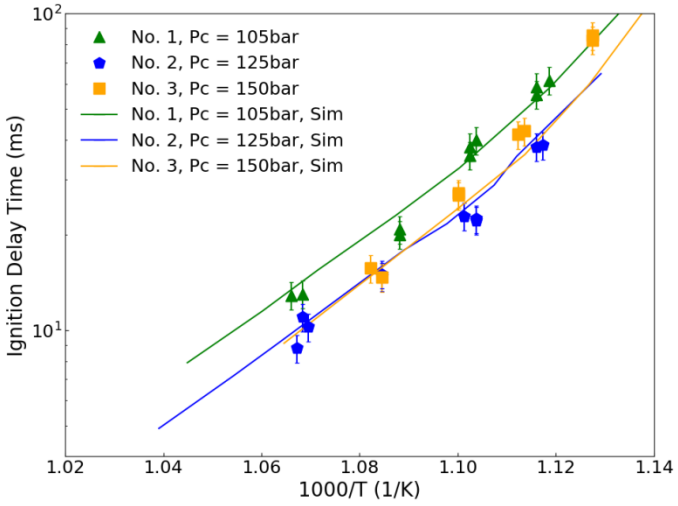

Figure 7: Comparison of experimental data (symbols) and model predictions (line) at varying pressures (105, 125 and 150 bar), ϕ = 0.526, with an inert gas dilution of 77.26%. The numbers in the legend (eg: No.1) represent the corresponding conditions in the test matrix.

The IDT data obtained from the experiments and simulations are plotted on a logarithmic scale as a function of inverse EOC temperature. **Figure 7** shows the experimental data and the simulation for 100% CH_4 at pressures of 105, 125, and 150 bar with 77.26% inert gas fraction. The reactivity increases as the pressure increases because of the increase in the concentration of the reactive species and this trend can be seen in the 105 and 125 bar data. In order to achieve higher EOC pressures, the compression ratio had to be increased for the 150 bar case and subsequently the ratio of diluent gases (Ar/N_2). This led to smaller compression volumes and different heat transfer coefficients ultimately leading to stronger heat loss and consequently longer IDTs for the 150 bar experiments. However, by using the volume profiles deduced from the non-reactive experiments, the differences are accounted for in the simulations and all of these shows good agreement with the experimental results, where the majority of the simulations are within the variation of the experimental results.

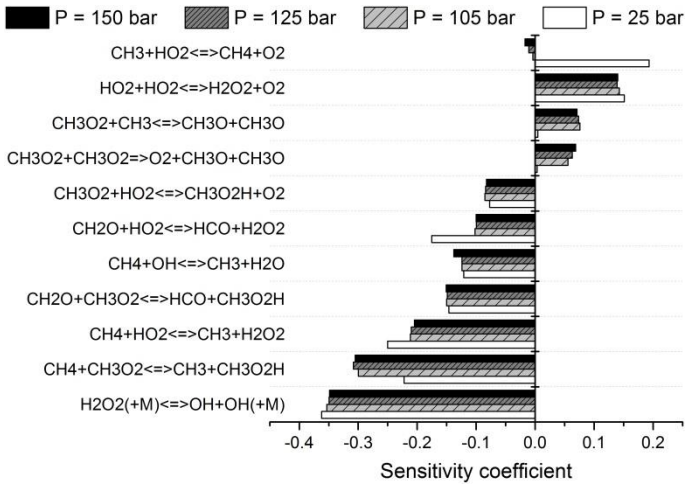

Figure 8: Brute force sensitivity analysis of IDT, ϕ = 0.526, T_c = 910 K, P_c = 25 bar, 105 bar, 125 bar, and 150 bar

To highlight the important reactions that affect the reactivity during the ignition process, a series of sensitivity analysis have been performed. **Figure 8** shows a brute force sensitivity analysis using Chemkin Pro at ϕ = 0.526, T_C = 910 K, P_C = 105 bar, 125 bar, 150 bar, and 25 bar. In the analysis, the rate constants of each reaction were increased and decreased by a factor of two (k_+ and k_-), and the simulations were performed using two mechanisms with these changes to derive the IDTs (τ_+ and τ_-). The sensitivity coefficient (S) is defined as:

$$S = \frac{\ln(\tau_+/\tau_-)}{\ln(k_+/k_-)} = \frac{\ln(\tau_+/\tau_-)}{\ln(2/0.5)}$$

Therefore, a reaction with a positive sensitivity coefficient inhibits reactivity while that with a negative sensitivity coefficient promotes reactivity.

At higher pressures (105 bar, 125 bar, and 150 bar) the most sensitive reactions remain the same. The sensitivity factors of each reaction under these different pressures are also similar; however, at lower pressures, some more significant changes can be observed. Under all four conditions, the decomposition of H_2O_2 is the most sensitive reaction, which promotes reactivity by producing two ȮH radicals. On the other hand, the chain termination reaction $H\dot{O}_2 + H\dot{O}_2 = H_2O_2 + O_2$ is in all cases one of the most inhibiting reactions. This is because one $H\dot{O}_2$ radical could be otherwise converted into H_2O_2 by abstracting one hydrogen atom from CH_4 or CH_2O. Thus $H\dot{O}_2$ is a critical species in the ignition process of methane at the current high-pressure conditions. According to the rate of production analysis, $H\dot{O}_2$ is mainly produced from the reaction of oxygen with radicals including $H\dot{C}O$, $CH_3\dot{O}$, and Ḣ atom, all of which result from the oxidation

285 of $\dot{C}H_3$ radical via the sequence of $CH_3\dot{O}_2 \rightarrow CH_3O_2H \rightarrow CH_3\dot{O} \rightarrow CH_2O \rightarrow H\dot{C}O$. The decomposition of CH_3O_2H
286 is another important chain branching reaction that produces a $\dot{O}H$ radical and a $CH_3\dot{O}$ radical. This reaction is
287 not shown in **Figure 8** as sensitive, due to its high rates under all considered conditions. However, several
288 reactions producing CH_3O_2H from its precursor, $CH_3\dot{O}_2$ radical, are found to be sensitive in promoting
289 reactivity as shown in **Figure 8,** while the competing reactions inhibit reactivity.

290 Amongst the most sensitive reactions shown in **Figure 8** the decomposition of H_2O_2 is the only reaction
291 in the current mechanism whose rate constants include a fall-off behaviour. This means that, at lower
292 pressures, H_2O_2 decomposes at a lower rate and therefore restricts the reactivity. Accordingly, it can be seen
293 in **Figure 8** that most reactions related to H_2O_2, either producing or consuming it, are more sensitive to lower
294 pressures. On the other hand, the other reactions are more sensitive at higher pressures. These reactions
295 mainly affect the production and consumption of $CH_3\dot{O}_2$ radical, which is the precursor of CH_3O_2H as
296 discussed above. This trend is more obvious in comparing the sensitivity analysis at higher pressures to the
297 one at 25 bar: the reactions that directly involve H_2O_2 are more sensitive under lower pressures while the
298 others are less sensitive. It needs to be noted that the most inhibiting reaction under 25 bar is the chain
299 termination reaction between $\dot{C}H_3$ and $H\dot{O}_2$, which is not sensitive under high pressures. This is because $\dot{C}H_3$
300 radical could add to O_2 more easily at high pressures and result in chain branching process as discussed
301 above. Overall this analysis shows that the ranking of reactivity controlling reactions changes at higher
302 pressures thereby underlining the importance of fundamental kinetic investigations at application relevant
303 pressures.

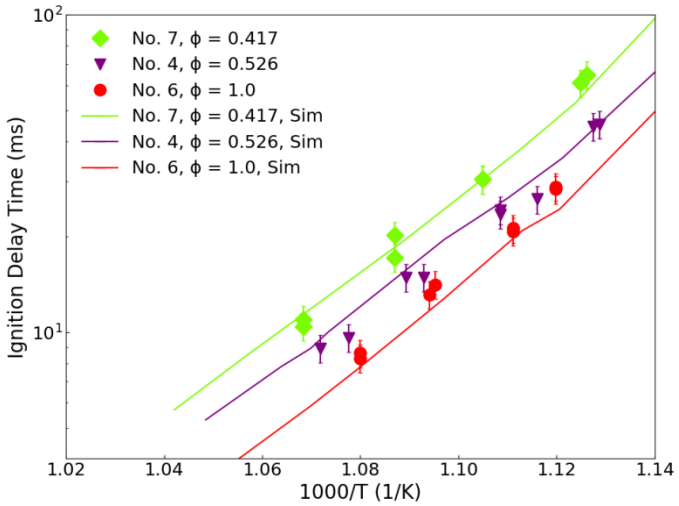

Figure 9: Comparison of experimental data (symbols) and model predictions (line) for variation of equivalence ratio (ϕ= 0.417, 0.526 and 1.0), at pressures of 125 and 160 bar with an inert gas dilution of 75.69, 74.86 and 80.13%.

Figure 9 depicts the effect of equivalence ratio on reactivity including both experimental results and model predictions. The conditions for equivalence ratio 0.417 and 0.526 are fuel/air mixtures, where the diluent proportions are varied to change the EOC temperature, whereas an equivalence ratio of 1.0 is a dilute condition with excess diluent equivalent to a 30% EGR condition. In this temperature regime, the reactivity of the mixture is strongly dependent on the concentration of the fuel, and as the mixture becomes rich the reactivity of the system increases. This is in agreement with previous studies [16, 28, 29]. The model captures the trends in reactivity very well.

Figure 10 illustrates the effect of the addition of ethane (13% mol) on reactivity at 125 bar and ϕ = 0.526. In general, in the low-temperature regimes (890–933 K), the reactivity increases with an increase in carbon chain length. This increase in carbon chain length facilitates the low-temperature chemistry paving the way for opportunities for isomerization reactions and further leading to chain branching reactions. Hence, the addition of ethane influences the low-temperature chemistry of the mixture, thereby increasing its reactivity. However, the experiments carried out for the CH_4/C_2H_6 blend were performed with a higher compression ratio and smaller EOC volumes. This leads to an increase in heat loss and consequently results in lower average temperatures and longer IDTs, which is more obvious in the lower temperature region of **Figure 10**. Again, the model captures the change in reactivity well.

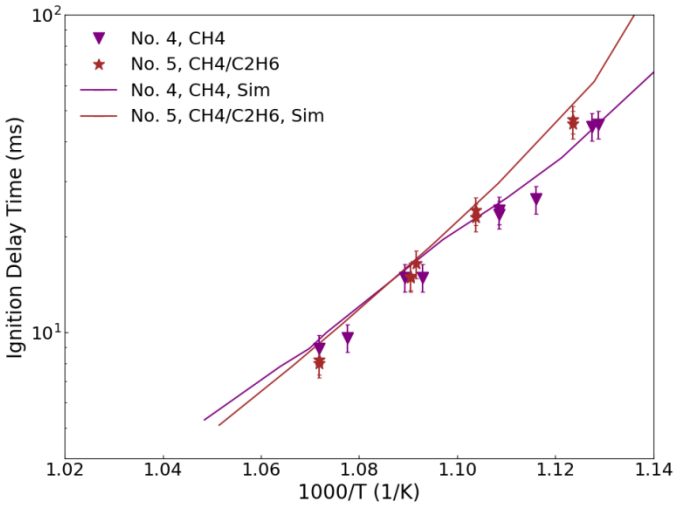

Figure 10: Comparison of experimental data (symbols) and model predictions (line) for variation of fuel mixtures at a pressure of 125bar, ϕ=0.526 and with an inert gas dilution of 74.86 and 75.21%.

In the preceding discussion, the addition of ethane promoted the reactivity of the system and shortens the IDTs. **Figure 11** shows a sensitivity analysis of reactions to IDTs with and without ethane addition to fuel mixture composition under the same conditions. The reactivity of the mixture and the sensitive reactions mostly remain the same because only 13% ethane was added. Amongst the top ten most sensitive reactions, there are three reactions involving C2 chemistry.

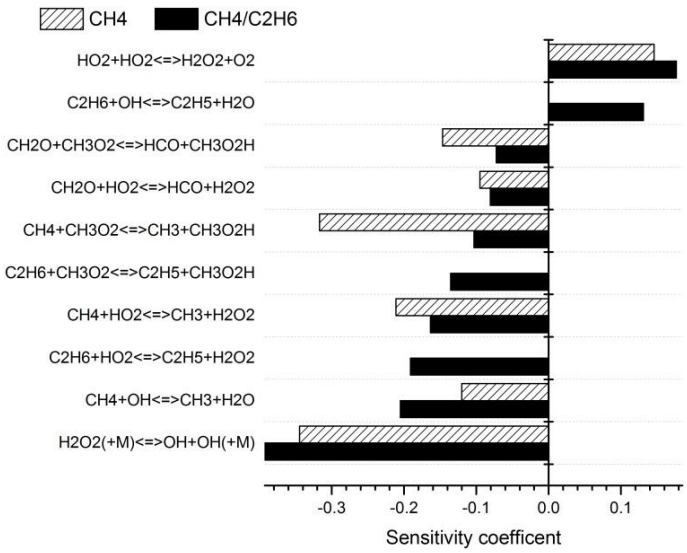

Figure 11: Brute force sensitivity analysis of ignition delay time, ϕ= 0.526, T = 910 K, P_c = 125 bar

Hydrogen atom abstraction from ethane by $H\dot{O}_2$ and $\dot{C}H_3O_2$ radicals producing H_2O_2 and CH_3O_2H promote reactivity. This trend is consistent with our analysis for conditions without ethane present: the reactions that

produce H_2O_2 and CH_3O_2H promote reactivity because these species are critical in leading to chain branching. On the other hand, H-atom abstraction from ethane by ȮH radicals inhibits reactivity, as this competes with CH_4 for ȮH radicals, which promotes reactivity. In general, the addition of ethane increases mixture reactivity. For ethane, hydrogen abstraction is easier than for methane because the ethane molecule has more (six as opposed to four) C–H bonds, which are relatively weaker than those of methane. Due to the presence of the beta carbon, ethyl can readily lose one hydrogen atom on the beta carbon via β-scission or hydrogen abstraction by O_2, producing ethylene and a hydrogen atom or hydroperoxyl radical. The production of Ḣ atoms and $HȮ_2$ radicals in this way leads to higher reactivity.

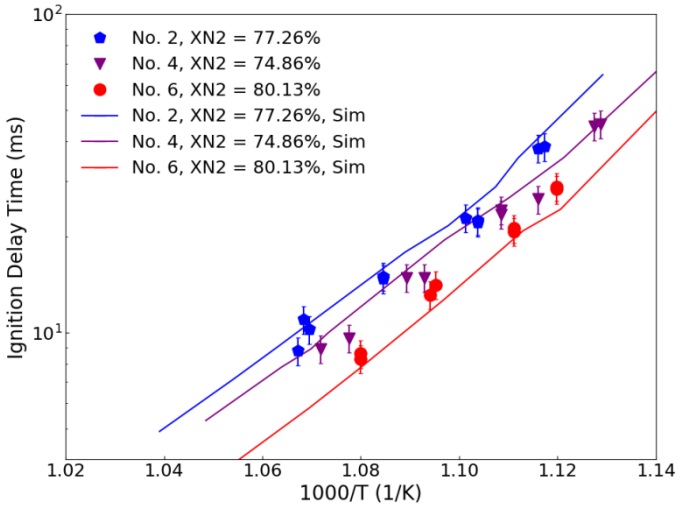

Figure 12: Comparison of experimental data (symbols) and model predictions (line) for methane mixtures at different dilution percentage at a pressure of 125 and 160 bar with ϕ = 0.526 & 1.0.

Finally, **Figure 12** highlights the effect of varying the inert gas fraction representing a varying EGR fraction as discussed earlier. Diluting the mixture decreases the concentration of the reactive components leading to longer IDTs. The inert gas fraction in the experiments is increased from 74.86% (0%) to 77.30% (10%) at 125 bar for fuel-lean mixtures, whereas for the stoichiometric conditions at 160 bar the inert gas fraction is 80.13%, representing a 30% dilution. The calculated ignition delay is consistent with the experimental data and captures the trend well. In general, for majority of the data sets the deviation of the model from the experiments is within the experimental variation, thereby showing that the chemical kinetic mechanism is able to predict the IDTs at the targeted regime of higher pressures and lower temperatures.

5. Conclusions

Within this study, a range of experimental data were acquired in an RCM for CH_4 and CH_4/C_2H_6 mixtures at varying equivalence ratios, dilution percentages, and pressures ranging from 105 to 160 bar in the temperature range of 845 - 940 K. Although there have been a number of studies on IDT measurements in the high and intermediate temperature regime, there is very limited data available in the literature at higher pressures in the RCM regime. The results of this study are the first set of data for CH_4 and CH_4/C_2H_6 mixtures at pressures from 105 to 160 bar taken to study knocking characteristics in application relevant conditions. An explicit description of the limitations of performing high-pressure experiments in an RCM and the approach used to overcome these limitations has been highlighted in this study. The load on the pressure sensor during the ignition event is reduced with the introduction of a recessed configuration. The issue of pre-ignition occurring during the experiments at these high-pressure conditions was resolved with the addition of a thin shim between the hydraulic and reaction chambers. Two dynamic pressure sensors have been used to complement the shortcomings of each other while the Kistler is limited by the pressure limit and the PCB is limited by its inability to account for the heat shock effect. The approach of using the pressures sensors in tandem to quantify the heat shock effect and determination of the compressed pressure is established. However, the problem of encountering oscillations at the end of compression so far limits our ability to achieve pressures higher than 160 bar. The recently published AramcoMech 2.0 was optimized and used to simulate the conditions in the test matrix. The mechanism not only captures the reactivity trends at various conditions of the matrix but also predicts quantitatively the measured IDTs. The majority of the IDT data is predicted within the variation of the experiments. The key reactions promoting and suppressing reactivity at these conditions were identified using a brute force sensitivity analysis. The decomposition of H_2O_2 producing two $\dot{O}H$ radicals seems to be the most sensitive reaction for all conditions, including both CH_4 and CH_4/C_2H_6 mixtures. The chain termination reaction of $\dot{C}H_3$ and $H\dot{O}_2$ suppresses the reactivity at lower pressures (25 bar), whereas at higher pressures (150 bar) it remains insensitive for the CH_4 mixtures. Moreover, the abstraction of hydrogen from ethane by $H\dot{O}_2$ and $CH_3\dot{O}_2$ radicals enhances the reactivity in CH_4/C_2H_6 mixtures. Overall, this study highlights the methodology for performing high-pressure

experiments in an RCM and also emphasizes the importance of the fundamental understanding of chemical kinetics at application relevant pressures.

Supplementary Material

1. Calculation: EGR % to N_2 dilution
2. Quantification of heat loss
3. Flat and Recessed configuration differences
4. Ignition delay time measurement data
5. Uncertainty Estimation
6. Constant volume simulations for the conditions in this study
7. Experimental Overview: non-reactive profiles
8. Comparison of the current mechanism, AramcoMech 1.3 and AramcoMech 2.0 mechanism
9. Mechanism file and thermal data. (separate files)
10. Non-Reactive profiles (separate folder)

Funding

This research did not receive any specific grant from funding agencies in the public, commercial, or non-for-profit sectors.

References

[1] B. Haake, J. Geiger, in: Spectrum - Technology highlights and R&D Activities at FEV, Special Edition Gas-operated drives, FEV, October 2013.

[2] B. Hüchtebrock, M. Umierski, J. Geiger, A. Dhongde, S. H., Ultra high specific load above 30 bar BMEP-is that reasonable?, WTZ Roßlau, Dessau, 2015.

[3] L.J. Spadaccini, M.B. Colket III, Ignition delay characteristics of methane fuels, Progress in Energy and Combustion Science, 20 (1994) 431-460.

[4] J. de Vries, E.L. Petersen, Autoignition of methane-based fuel blends under gas turbine conditions, Proc. Combust. Inst., 31 (2007) 3163-3171.

[5] J. Huang, W.K. Bushe, Experimental and kinetic study of autoignition in methane/ethane/air and methane/propane/air mixtures under engine-relevant conditions, Combust. Flame, 144 (2006) 74-88.

[6] J. Huang, P.G. Hill, W.K. Bushe, S.R. Munshi, Shock-tube study of methane ignition under engine-relevant conditions: experiments and modeling, Combust. Flame, 136 (2004) 25-42.

[7] E.L. Petersen, D.F. Davidson, R.K. Hanson, Ignition Delay Times of Ram Accelerator CH/O/Diluent Mixtures, Journal of Propulsion and Power, 15 (1999) 82-91.

[8] J. Herzler, C. Naumann, Shock-tube study of the ignition of methane/ethane/hydrogen mixtures with hydrogen contents from 0% to 100% at different pressures, Proc. Combust. Inst., 32 (2009) 213-220.

[9] E.L. Petersen, J.M. Hall, S.D. Smith, J. de Vries, A.R. Amadio, M.W. Crofton, Ignition of Lean Methane-Based Fuel Blends at Gas Turbine Pressures, Journal of Engineering for Gas Turbines and Power, 129 (2007) 937-944.

[10] E.L. Petersen, M. Röhrig, D.F. Davidson, R.K. Hanson, C.T. Bowman, High-pressure methane oxidation behind reflected shock waves, Proc. Combust. Inst., 26 (1996) 799-806.

[11] Y. Zhang, Z. Huang, L. Wei, J. Zhang, C.K. Law, Experimental and modeling study on ignition delays of lean mixtures of methane, hydrogen, oxygen, and argon at elevated pressures, Combust. Flame, 159 (2012) 918-931.

421 [12] V.P. Zhukov, V.A. Sechenov, A.Y. Starikovskii, Spontaneous Ignition of Methane–Air Mixtures in a Wide
422 Range of Pressures, Combustion, Explosion, and Shock Waves, 39 (2003) 487-495.
423 [13] R.S. Tranter, H.R. Amoorthy, A. Raman, K. Brezinsky, M.D. Allendorf, High-pressure single-pulse shock
424 tube investigation of rich and stoichiometric ethane oxidation, Proc. Combust. Inst., 29 (2002) 1267-1275.
425 [14] C.J. Goy, A.J. Moran, G.O. Thomas, Autoignition characteristics of gaseous fuels at representative gas
426 turbine conditions, ASME International gas turbine & aeroengine technical congress, 2001.
427 [15] N. Lamoureux, C.E. Paillard, Natural gas ignition delay times behind reflected shock waves: Application
428 to modelling and safety, Shock Waves, 13 (2003) 57-68.
429 [16] C.J. Aul, W.K. Metcalfe, S.M. Burke, H.J. Curran, E.L. Petersen, Ignition and kinetic modeling of methane
430 and ethane fuel blends with oxygen: A design of experiments approach, Combust. Flame, 160 (2013) 1153-
431 1167.
432 [17] T. Asaba, K. Yoneda, N. Kakihara, T. Hikita, A shock tube study of ignition of methane-oxygen mixtures,
433 Symposium (International) on Combustion, 9 (1963) 193-200.
434 [18] D.F. Cooke, A. Williams, Shock tube studies of methane and ethane oxidation, Combustion and Flame,
435 24 (1975) 245-256.
436 [19] H. Miyama, T. Takeyama, Mechanism of Methane Oxidation in Shock Waves, The Journal of Chemical
437 Physics, 40 (1964) 2049-2050.
438 [20] T. Tsuboi, H.G. Wagner, Homogeneous thermal oxidation of methane in reflected shock waves,
439 Symposium (International) on Combustion, 15 (1975) 883-890.
440 [21] A. Lifshitz, K. Scheller, A. Burcat, G.B. Skinner, Shock-tube investigation of ignition in methane-oxygen-
441 argon mixtures, Combustion and Flame, 16 (1971) 311-321.
442 [22] H. El Merhubi, A. Kéromnès, G. Catalano, B. Lefort, L. Le Moyne, A high pressure experimental and
443 numerical study of methane ignition, Fuel, 177 (2016) 164-172.
444 [23] S. Heyne, A. Roubaud, M. Ribaucour, G. Vanhove, R. Minetti, D. Favrat, Development of a natural gas
445 reaction mechanism for engine simulations based on rapid compression machine experiments using a multi-
446 objective optimisation strategy, Fuel, 87 (2008) 3046-3054.

447 [24] D. Healy, H.J. Curran, J.M. Simmie, D.M. Kalitan, C.M. Zinner, A.B. Barrett, E.L. Petersen, G. Bourque,
448 Methane/ethane/propane mixture oxidation at high pressures and at high, intermediate and low
449 temperatures, Combust. Flame, 155 (2008) 441-448.
450 [25] D. Healy, D.M. Kalitan, C.J. Aul, E.L. Petersen, G. Bourque, H.J. Curran, Oxidation of C1−C5 Alkane
451 Quinternary Natural Gas Mixtures at High Pressures, Ener. Fuels, 24 (2010) 1521-1528.
452 [26] S. Gersen, N.B. Anikin, A.V. Mokhov, H.B. Levinsky, Ignition properties of methane/hydrogen mixtures in
453 a rapid compression machine, International Journal of Hydrogen Energy, 33 (2008) 1957-1964.
454 [27] S. Gersen, A.V. Mokhov, J.H. Darmeveil, H.B. Levinsky, P. Glarborg, Ignition-promoting effect of NO2 on
455 methane, ethane and methane/ethane mixtures in a rapid compression machine, Proc. Combust. Inst., 33
456 (2011) 433-440.
457 [28] S. Gersen, H. Darmeveil, H. Levinsky, The effects of CO addition on the autoignition of H2, CH4 and
458 CH4/H2 fuels at high pressure in an RCM, Combust. Flame, 159 (2012) 3472-3475.
459 [29] U. Burke, K.P. Somers, P. O'Toole, C.M. Zinner, N. Marquet, G. Bourque, E.L. Petersen, W.K. Metcalfe, Z.
460 Serinyel, H.J. Curran, An ignition delay and kinetic modeling study of methane, dimethyl ether, and their
461 mixtures at high pressures, Combust. Flame, 162 (2015) 315-330.
462 [30] R.F. Pachler, A.K. Ramalingam, K.A. Heufer, F. Winter, Reduction and validation of a chemical kinetic
463 mechanisms including necessity analysis and investigation of CH_4/C_3H_8 oxidation at pressures up to 120 bar
464 using a Rapid Compression Machine, Fuel, (2015 (Submitted)).
465 [31] N. Donohoe, K.A. Heufer, C.J. Aul, E.L. Petersen, G. Bourque, R. Gordon, H.J. Curran, Influence of steam
466 dilution on the ignition of hydrogen, syngas and natural gas blends at elevated pressures, Combustion and
467 Flame, 162 (2015) 1126-1135.
468 [32] W. Zeng, H. Ma, Y. Liang, E. Hu, Experimental and modeling study on effects of N2 and CO2 on ignition
469 characteristics of methane/air mixture, Journal of Advanced Research, 6 (2015) 189-201.
470 [33] C. Lee, S. Vranckx, K.A. Heufer, V. Khomik Sergey, Y. Uygun, H. Olivier, X. Fernandez Ravi, On the
471 Chemical Kinetics of Ethanol Oxidation: Shock Tube, Rapid Compression Machine and Detailed Modeling
472 Study, in: Z. Phys. Chem., 2012, pp. 1.

473 [34] J. Würmel, E.J. Silke, H.J. Curran, M.S. Ó Conaire, J.M. Simmie, The effect of diluent gases on ignition
474 delay times in the shock tube and in the rapid compression machine, Combust. Flame, 151 (2007) 289-302.
475 [35] C. Morley, Gaseq, in, available at <http://www.gaseq.co.uk/>.
476 [36] B.W. Weber, C.-J. Sung, M.W. Renfro, On the uncertainty of temperature estimation in a rapid
477 compression machine, Combustion and Flame, 162 (2015) 2518-2528.
478 [37] S.M. Burke, U. Burke, R. Mc Donagh, O. Mathieu, I. Osorio, C. Keesee, A. Morones, E.L. Petersen, W.
479 Wang, T.A. DeVerter, M.A. Oehlschlaeger, B. Rhodes, R.K. Hanson, D.F. Davidson, B.W. Weber, C.-J. Sung, J.
480 Santner, Y. Ju, F.M. Haas, F.L. Dryer, E.N. Volkov, E.J.K. Nilsson, A.A. Konnov, M. Alrefae, F. Khaled, A. Farooq,
481 P. Dirrenberger, P.-A. Glaude, F. Battin-Leclerc, H.J. Curran, An experimental and modeling study of propene
482 oxidation. Part 2: Ignition delay time and flame speed measurements, Combust. Flame, 162 (2015) 296-314.
483 [38] G. Mittal, C.-J. Sung, Autoignition of toluene and benzene at elevated pressures in a rapid compression
484 machine, Combustion and Flame, 150 (2007) 355-368.
485 [39] Y. Li, C.-W. Zhou, K.P. Somers, K. Zhang, H.J. Curran, The oxidation of 2-butene: A high pressure ignition
486 delay, kinetic modeling study and reactivity comparison with isobutene and 1-butene, Proceedings of the
487 Combustion Institute, 36 (2017) 403-411.
488 [40] W.K. Metcalfe, S.M. Burke, S.S. Ahmed, H.J. Curran, A Hierarchical and Comparative Kinetic Modeling
489 Study of C1 − C2 Hydrocarbon and Oxygenated Fuels, International Journal of Chemical Kinetics, 45 (2013)
490 638-675.
491 [41] Z. Hong, K.-Y. Lam, R. Sur, S. Wang, D.F. Davidson, R.K. Hanson, On the rate constants of OH + HO2 and
492 HO2 + HO2: A comprehensive study of H2O2 thermal decomposition using multi-species laser absorption,
493 Proc. Combust. Inst., 34 (2013) 565-571.
494 [42] U. Burke, W.K. Metcalfe, S.M. Burke, K.A. Heufer, P. Dagaut, H.J. Curran, A Detailed Chemical Kinetic
495 Modeling, Ignition Delay time and Jet-Stirred Reactor Study of Methanol Oxidation, Combust. Flame, (2015).
496 [43] J. Aguilera-Iparraguirre, H.J. Curran, W. Klopper, J.M. Simmie, Accurate Benchmark Calculation of the
497 Reaction Barrier Height for Hydrogen Abstraction by the Hydroperoxyl Radical from Methane. Implications
498 for CnH2n+2 where n = 2 → 4, J. Phys. Chem. A, 112 (2008) 7047-7054.

499 [44] C.-J. Sung, H.J. Curran, Using rapid compression machines for chemical kinetics studies, Progress in
500 Energy and Combustion Science, 44 (2014) 1-18.

501